



EXPERIMENTAL INVESTIGATION OF THE EFFECT OF THE LONGITUDINAL REINFORCEMENT CONTENT OF RING BEAMS ON THE CYCLIC BEHAVIOR OF MASONRY SPANDRELS

A. Dazio¹ and K. Beyer²

Abstract

In many unreinforced masonry (URM) buildings reinforced concrete (RC) ring beams are introduced at each storey in order to maintain the integrity of the building when subjected to seismic loading. Such ring beams also contribute to the in-plane resistance of URM walls consisting of vertical piers connected by ring beams and often also by horizontal URM spandrels. The entity of the RC ring beam and the URM spandrel is in the following referred to as composite spandrel. Although numerical simulations have shown that composite spandrels have a significant influence on the seismic behavior of URM walls, their contribution has often been neglected since fundamental experimental evidence on the cyclic behavior of spandrel beams was lacking.

The paper discusses important phenomena affecting the cyclic force-deformation behavior observed during full-scale quasi-static cyclic tests on composite spandrels. In particular the effect of the longitudinal reinforcement content of the RC ring beam on the interaction between URM spandrel and RC ring beam as well as on stiffness, strength and deformation capacity of the composite spandrel are discussed. Based on the test results, first recommendations concerning the design and analysis of RC ring beams in URM structures are presented.

Introduction

Reinforced concrete (RC) ring beams are beams running around the circumference of an unreinforced masonry building (URM). In new URM buildings without RC floors such ring

¹ EUCENTRE, 27100 Pavia, Italy, alessandro.dazio@eucentre.it

² Ecole polytechnique fédérale de Lausanne (EPFL), 1015 Lausanne, Switzerland, katrin.beyer@epfl.ch

beams are typically introduced at each storey level [OPCM 2003, 2005]. Provided the ring beams are well connected to the masonry, the ring beams maintain the integrity of the buildings when subjected to seismic loading by connecting separate or orthogonal walls. They also allow at least a limited redistribution of the lateral forces between walls that act in one plane. Moreover, the ring beam provides a restraint to walls that are loaded out-of-plane, hence reducing the free height of the out-of-plane loaded wall. Ring beams also contribute to the in-plane stiffness and strength of spandrels which couple individual URM walls.

This paper investigates the contribution of the ring beams to the strength of the spandrel elements that couple the URM piers. The study is based on the results of an experimental programme on coupling elements consisting of a RC ring beam and a masonry spandrel, in the following abbreviated to “composite spandrel”. The composite spandrel test units were tested by the authors at full scale under quasi-static monotonic and cyclic loading at the structural engineering’s laboratory of the ETH Zurich [Beyer 2010a]. The paper commences with a short presentation of the experimental programme and continues with an evaluation of the behavior of composite spandrels with RC beams with different longitudinal reinforcement contents.

Experimental programme

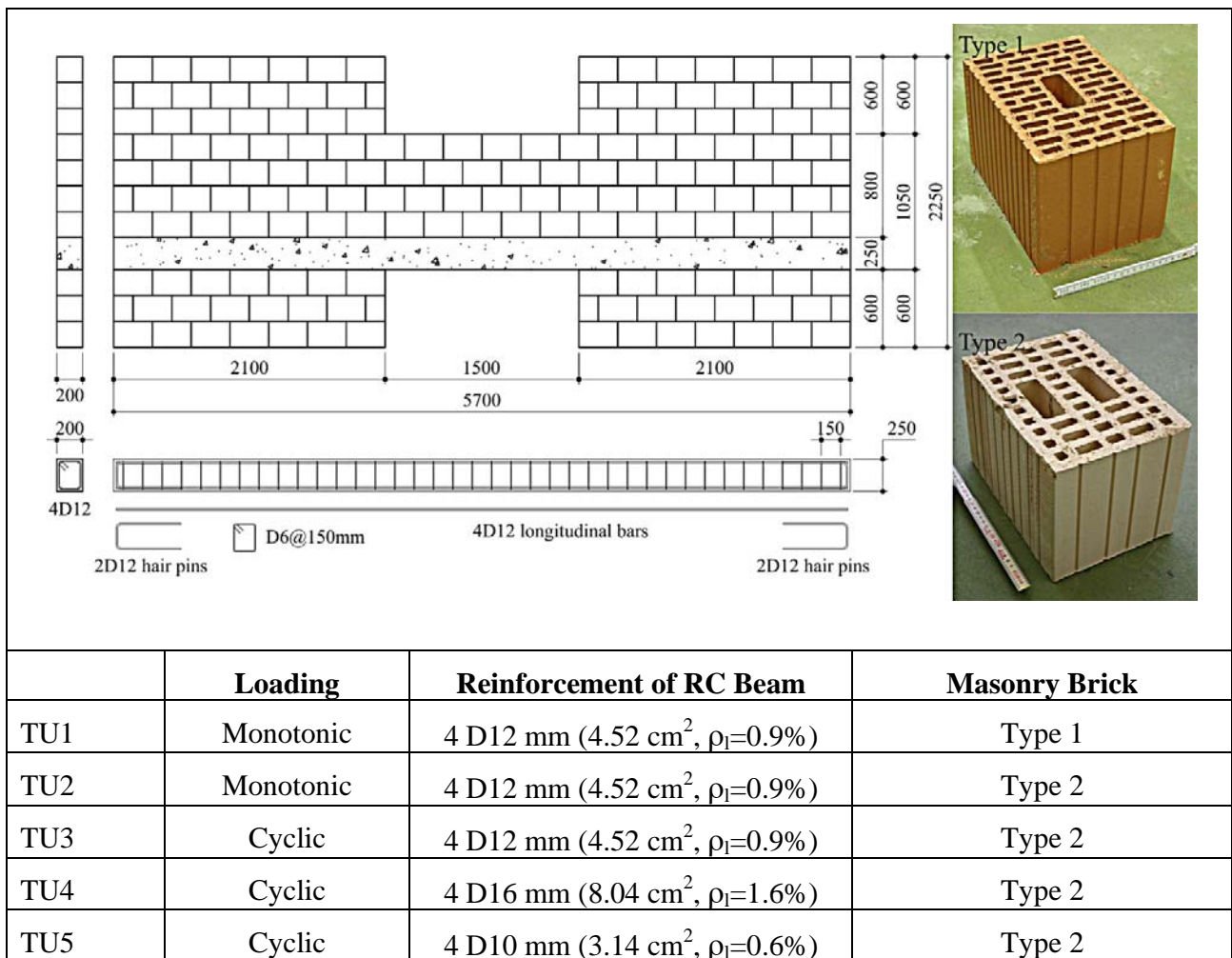
The test programme was initiated by the first author recognizing that the experimental data basis on such elements was very scarce, therefore preventing the validation of numerical models and design approaches for spandrel elements. Within the test programme, five composite spandrels and four masonry spandrels were tested. The masonry spandrel elements represented spandrel elements in buildings without RC floor or ring beam and featured either a timber lintel or a shallow masonry arch to bridge the opening [Beyer 2010a,b]. The composite spandrels featured a masonry spandrel and a RC beam, which can either represent a RC ring beam or a strip of a RC slab. In the following, only the part of the test programme will be outlined that concerned the composite spandrels.

Test units

Five composite spandrel test units with identical outer dimensions were tested. The dimensions of the test units are shown in Table 1. The table also lists for all test units the type of loading, the longitudinal reinforcement of the RC beam and the type of bricks that was used for the construction of the test unit. The parameters investigated were (i) the brick type, (ii) the loading scheme (monotonic / cyclic) and (iii) the longitudinal reinforcement content. The latter parameter is the topic discussed in this paper. The test units, for which the longitudinal reinforcement content was changed, are test units TU3, TU4 and TU5. The longitudinal reinforcement of TU3 consisted of 4 D12 mm bars. The Italian seismic design code [OPCM 2003, 2005] requires for RC ring beams a minimum longitudinal reinforcement area of 8 cm^2 , which corresponds to 4 D16 mm bars, and a minimum beam width equal to the width of the masonry wall. For the shear reinforcement a minimum of D6 mm hoops every 250 mm must be provided. TU4 therefore satisfies all the minimum requirements of a ring

beam according to OPCM 3431 [OPCM 2005]; only the shear reinforcement was with D6 mm hoops every 150 mm slightly larger than required. According to the European Seismic Design Code EC8 [CEN 2004] a ring beam has to be fitted with a minimum longitudinal reinforcement area of 2 cm^2 ; this is considerably smaller than the reinforcement area of TU1-4. For this reason a fifth spandrel was tested with a smaller longitudinal reinforcement of the RC beam (TU5). In parallel to the spandrel tests, material tests on reinforcement bars, concrete, mortar, bricks and small masonry wallettes were carried out [Beyer 2010a].

Table 1. Composite spandrels: Loading scheme, reinforcement and brick details for the five test units.



Test setup

Each test unit comprised the spandrel element which was framed by two piers (Table 1). In the test stand, the piers stood on two stiff beams (“lever beams”) that were supported on hinges at the centre line of the piers and connected to servo-hydraulic actuators at their ends (Figures 1 and 2). During testing the two servo-hydraulic actuators were moved with the same velocity in opposite directions. As a result, the two horizontal lever beams rotated and

the piers right and left to the spandrel were subjected to the same drifts, which caused the demand on the spandrel. The support of the South lever beam allowed next to a rotation also a sliding movement along the longitudinal axis of the beam. Hence, the test stand did not restrain the axial elongation of the spandrel. The two piers were post-tensioned by four vertical rods each. The forces in the vertical rods were kept constant throughout the test. The purpose of these rods was to simulate the axial force in piers in real buildings. However, it should be noted that the piers in the test units were not subjected to realistic moment and shear demands. The goal of the test campaign was not to test the piers but to test the spandrels.

Instrumentation

Different global and local quantities were measured during testing by means of hard-wired instruments. These included: (i) The actuator forces and the reaction forces at the supports of the beams, (ii) global deformation quantities, i.e. the rotation of the lever beams and the sliding movement of the South lever beam, (iii) the curvature and axial strain distribution along the RC beam and (iv) the forces in the vertical rods generating the axial load in the piers. From the measurements of the actuator forces and the forces at the supports, the shear force in the spandrel was computed. The rotation of the piers was measured by the linear variable differential transformers (LVDTs) mounted underneath the lever beams. The demand on the spandrel does not only depend on the pier rotations but also on the length of the spandrel. A “spandrel displacement” was computed as [Milani 2009]:

$$\Delta_{sp} = \theta \cdot (l_{sp} + l_{pier}) \quad [1]$$

Where l_{sp} is the length of the spandrel and l_{pier} the length of the pier. For the tested spandrels, these lengths were 1.50 m and 2.10 m, respectively. In addition to the hard-wired instruments, an optical measurement system (Optotrak Certus HD, [NDI 2009]) was used to measure the local deformations of the test unit. The system worked with a position sensor consisting of three cameras, which measured the 3D-coordinates of LEDs glued onto the test unit and base plates (Figure 1). The results of the optical measurements are still to be evaluated in detail and are therefore not yet included in this paper.

Effect of the longitudinal reinforcement content on the behavior of composite spandrels

The effect of the longitudinal reinforcement content of the RC beam on the behavior of the composite spandrel will be discussed using test units TU3, TU4 and TU5 as an example. All test units were tested under quasi-static cyclic loading and differed only concerning the longitudinal reinforcement content of the RC beam (Table 1). The effect of the longitudinal reinforcement content of the RC beam will be discussed with regard to the failure mechanism, the force and deformation capacity of the spandrel, the properties of the hysteresis curves and the curvature demand on the RC beam.



Figure 1. Photo of the test setup. View from the East.

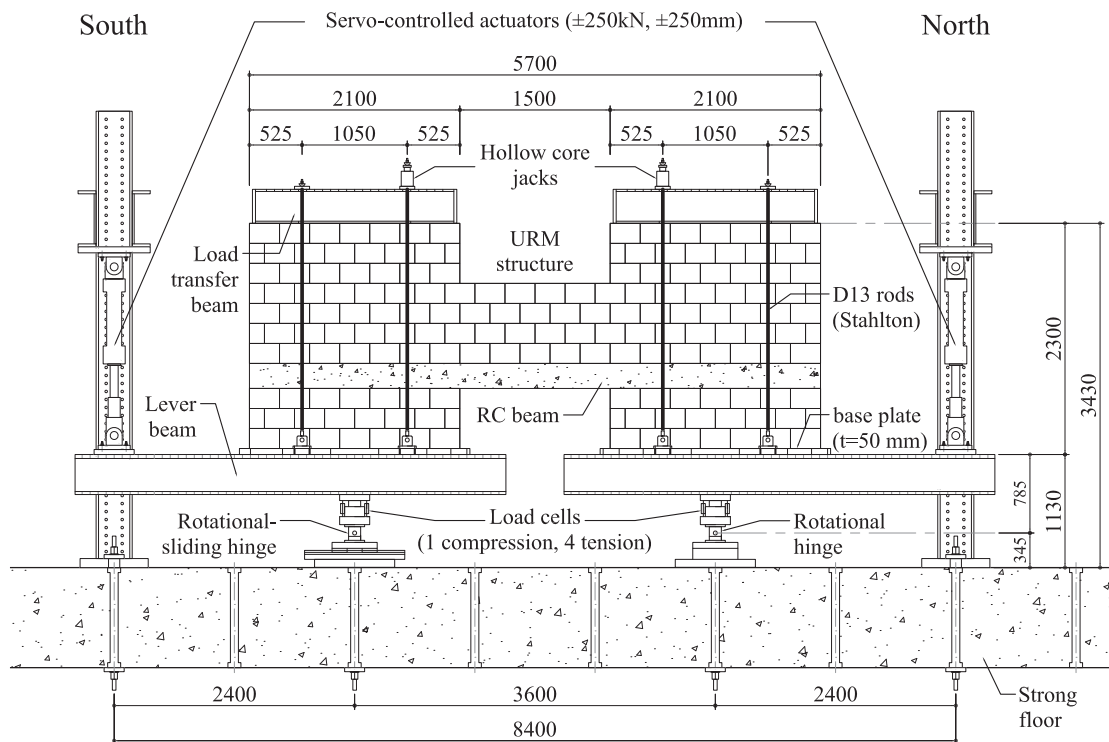


Figure 2. Drawing of the test setup for the composite spandrel. View from the East without side restraint. All dimensions are in [mm].

Failure Mechanisms

For the three test units, two different mechanisms could be identified, which are depicted in Figure 3. For low longitudinal reinforcement ratios (TU5) the initial crack pattern of the masonry spandrel and the RC beam suggested that a compression strut formed in the masonry spandrel, which was supported by a positive plastic hinge in the RC beam (Figure 3a). Hence, the positive plastic hinge in the RC beam formed not at the end of the spandrel – as one would conclude if the masonry spandrel would be neglected – but within the spandrel. The negative plastic hinge in the RC beam, on the contrary, formed at the end of the spandrel. A further difference of the two plastic hinges concerned their length: While the negative plastic hinge was rather short the South plastic hinge was typically spread over a longer part of the RC beam. At the onset of crushing of the compression diagonal in the masonry spandrel, the positive plastic hinge tended to move outwards towards the end of the spandrel. Almost all cracks that formed in the RC beam were near vertical flexural cracks. However, as the global deformations increased, local plastic deformations of the longitudinal beam reinforcement concentrated mainly in one single crack per hinge. The increasing width of these cracks led to a reduction of the shear capacity of the concrete due to reduced aggregate interlocking and hence to an increase of the local shear deformations. Shear failure did, however, not occur and final failure was due to rupture of the two bottom longitudinal reinforcement bars in the South hinge.

TU4 had the largest longitudinal reinforcement ratio. For the initial vertical stress level in the piers ($\sigma=0.4$ MPa), which was also applied to the piers of TU3 and TU5, the RC beam was so strong that, instead of the formation of a positive plastic hinges in the RC beam, the beam rocked on the pier, i.e. a gap between pier and the bottom of the RC beam opened up over the entire length of the pier (Figure 3b). The negative plastic hinges formed for larger rotation demands. From tests on masonry piers it is known that such a rocking mechanism has a very large deformation capacity [Frumento 2009]. To investigate the strength of the spandrel when plastic hinges formed, the axial stress in the piers was increased by 50% to $\sigma=0.6$ MPa. As a consequence, the gap between pier and RC beam did not open as much and the RC beam had to deform more. This increased deformation demand on the RC beam led to yielding of the positive plastic hinge and already in the second cycle to shear failure of the RC beam.

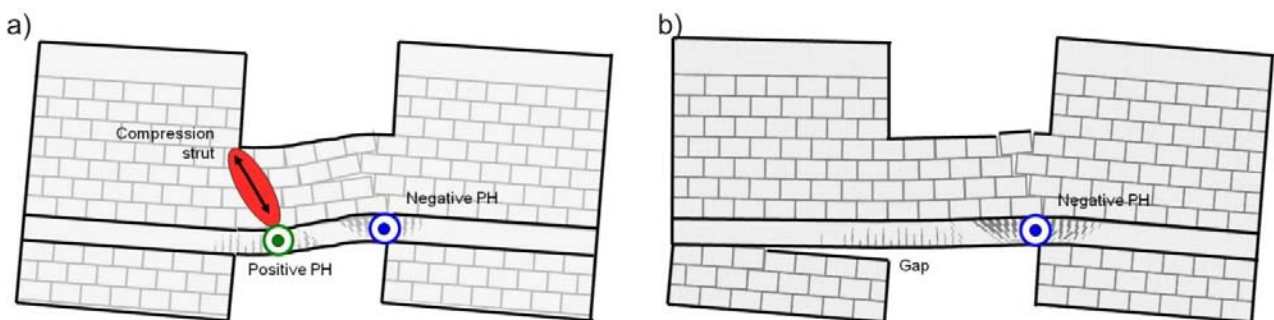


Figure 3. Mechanical models based on observed crack pattern: Mechanism with two plastic hinges in RC beam (a) and rocking mechanism with a negative plastic hinge only (b).

TU3 had an intermediate longitudinal reinforcement ratio. The mechanism that formed was a combination of the two mechanisms depicted in Figure 3, i.e. the gap between RC beam and pier opened up to some extent but the positive plastic hinge in the RC beam still formed. When compared to TU5 the compression struts in the masonry were subjected to significantly more damage (Figure 4). As the compression diagonals crushed the positive plastic hinges moved outwards towards the end of the spandrel. Since the shear reinforcement was the same for all test units, TU3 was more shear critical than TU5. As a consequence it finally failed within the positive plastic hinge in shear. When the direction of loading was reversed thereafter, also a longitudinal bar fractured within the positive plastic hinge.

The comparison of the failure mechanisms shows that the longitudinal reinforcement content affects the mechanism that formed, the damage to the masonry spandrel and therefore also the location of the plastic hinges in the RC beam. Since only the longitudinal reinforcement content was changed between the test units, the RC beams became prone to shear failure for an increased longitudinal reinforcement content.

Force and Deformation Capacity

The hysteresis curves of the test units are shown in the right column of Figure 4. The curves show on their y-axis the shear force in the spandrel, on their lower x-axis the rotation of the piers and on their upper x-axis the spandrel deformation according to Equation [1]. Figure 5 shows the envelope curves for the first and second cycles.

In general, the force-capacity of the spandrel increases as the longitudinal reinforcement increases. However, if the reinforcement content is sufficiently large to cause the rocking mechanism (Figure 3b), the capacity of the spandrel is a function of the axial force in the piers. This applied to TU4, when the axial stress in the piers was $\sigma=0.4$ MPa.

The envelope curves of TU3 and TU5 show that after reaching the peak strength, the strength degradation was less pronounced for TU5, which had a lower reinforcement content. As outlined above, the strength degradation is most likely associated with crushing of the compression strut which was more significant for TU3 than for TU5. TU4 shows no strength degradation at all, a fact which is due to the rocking mechanism where the “yield plateau” is not due to material nonlinearities but due to geometric properties. The small increases towards the end of the envelope curves of TU4 were due to a slight increase in axial force in the piers. The axial force in the piers was kept constant by means of hollow-core jacks connected to a load follower but as the gap between RC beam and pier became very wide, some of the jacks reached their end-stroke leading therefore to an increase in axial force in the piers. As the axial force increased the rocking strength increased.

When comparing the deformation capacity between the test units one should keep in mind that (i) the failure mechanisms were different and that (ii) for TU4 at $\delta=2.0\%$ the axial stress in the piers was increased to $\sigma=0.6$ MPa. If TU4 had been continued to be tested with $\sigma=0.4$ MPa, the rocking mechanism might have allowed to reach very large deformation capacities.

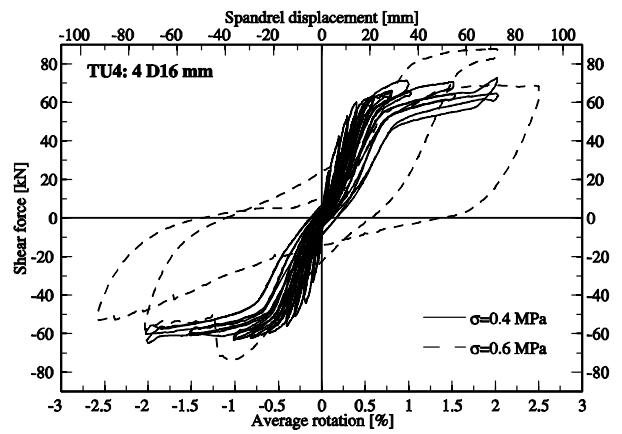
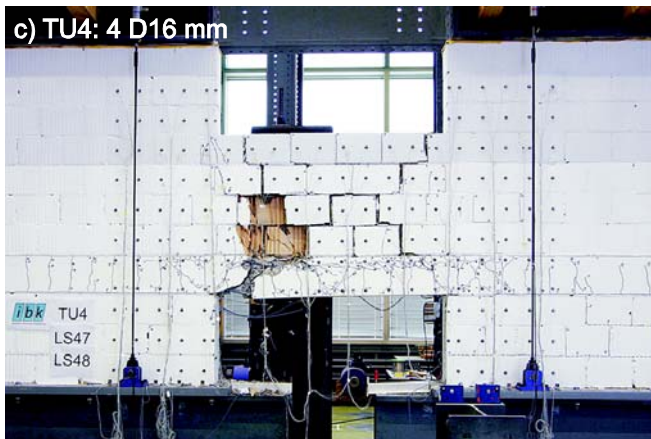
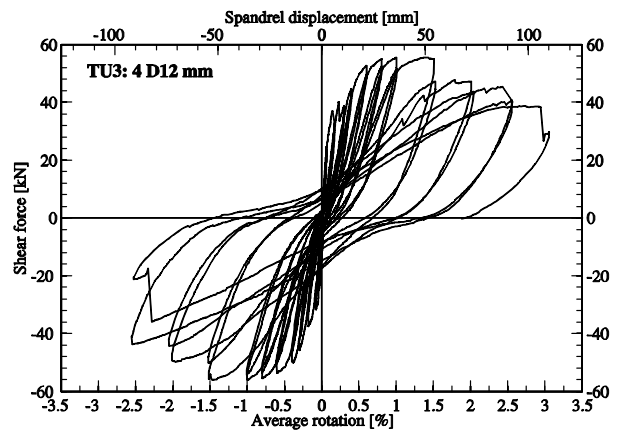
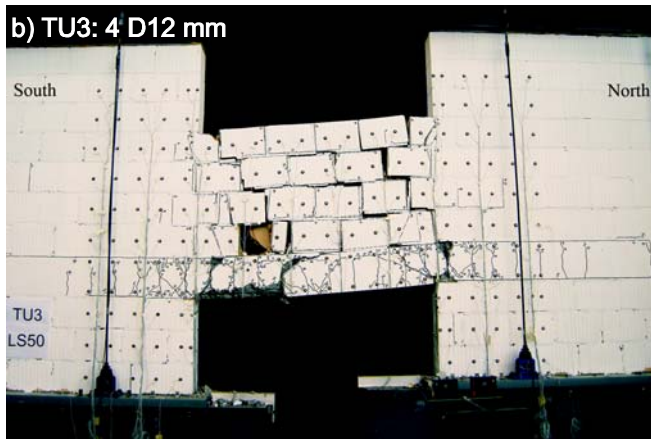
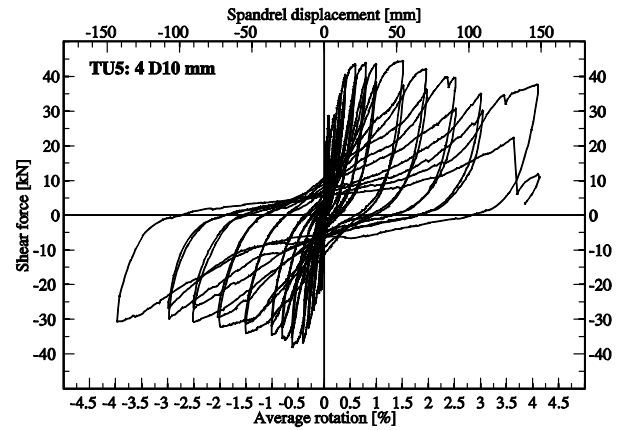
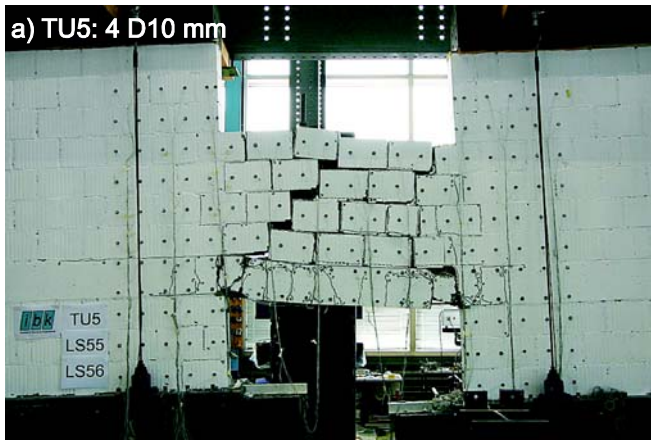


Figure 4. Test units with different longitudinal reinforcement contents of the RC beam: Crack pattern at failure and force-rotation hysteresis.

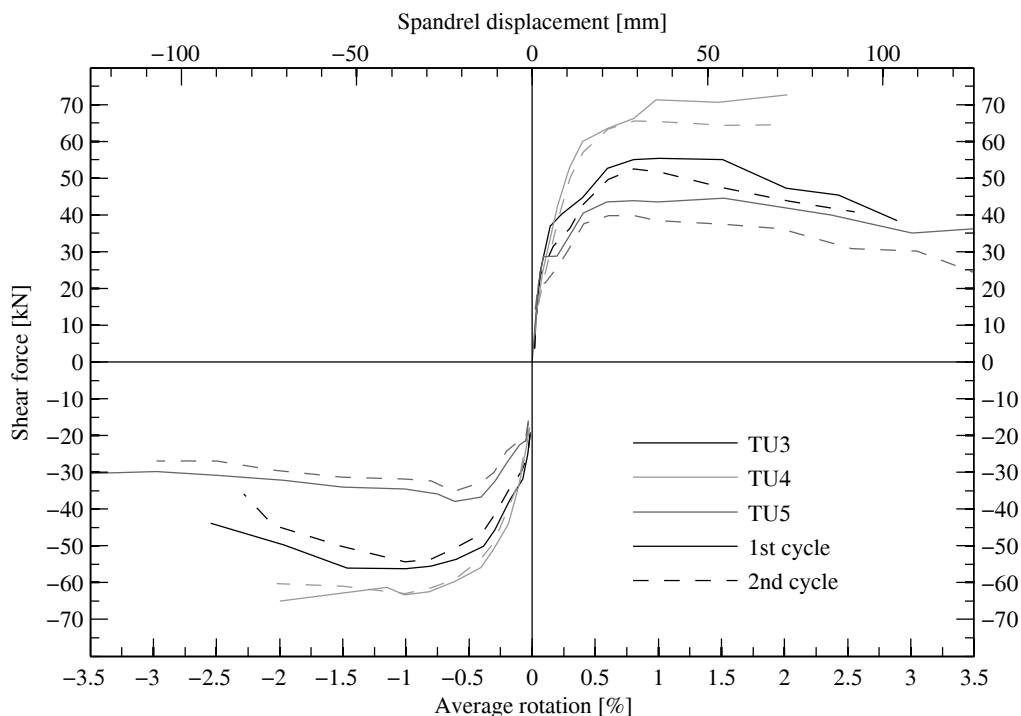


Figure 5. Envelope of the force-rotation hysteresis curves (for TU4 only those cycles with $\sigma=0.4$ MPa are included).

Hysteresis curves

Figure 6 shows the shape of the hysteresis loops using the cycles with peak rotations of 0.8% as an example ($\delta=0.8\%$ is the drift limit according to EC8, Part 3 [CEN 2005] for flexural failure of URM piers corresponding to significant damage). To display the loops at a similar size, the spandrel shear force was normalised by its absolute peak force recorded during the entire test. Due to the rocking mechanism the hysteresis loops of TU4 differ significantly from those of TU3 and TU5. The hysteretic energy of the rocking mechanism is noticeably smaller when compared to those of TU3 and TU5. The shapes of the hysteresis loops of TU3 and TU5 are rather similar, although the hysteresis loop of TU5 is a little fatter than that of TU3. The reason could be related to the fact that for the same pier rotation, the curvature demand on the RC beam of TU5 is larger than the curvature demand of TU3. TU3 exhibited a mixed mechanism incorporating some opening of the gap between the bottom of the RC beam and the pier, which reduced the rotation demand on the RC beam.

Curvature demand on RC beam

Figure 7 shows the curvature distribution along the RC beam, which was derived from measurements stemming from two chains of LVDTs located at the top and bottom of the RC beam. The load steps represented in Figure 7 correspond to the positive and negative peaks of the first cycles of a particular rotation level. The yield curvature was estimated using the following equation [Priestley 2007]:

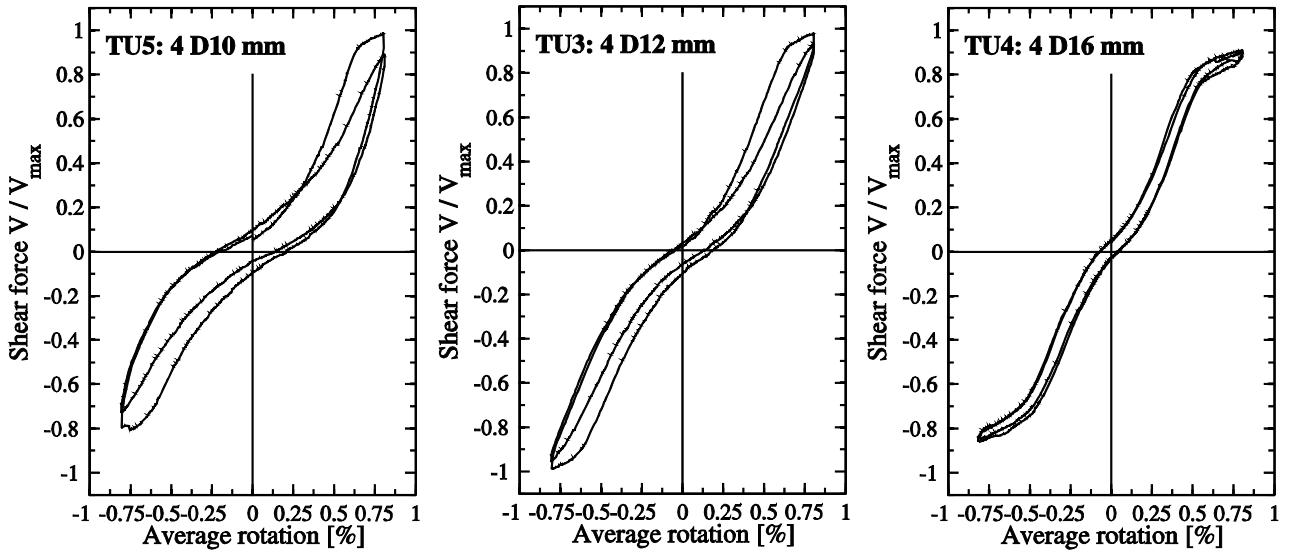


Figure 6. Shape of the hysteresis loops for the cycles with peak drifts of 0.8%. The shear force is normalized by the maximum absolute shear force measured for all cycles with $\sigma=0.4$ MPa.

$$\varphi_y = 2.0 \frac{\varepsilon_{sy}}{h_b} \quad [2]$$

where ε_{sy} is the yield strain of the longitudinal reinforcement and h_b the height of the RC beam. A positive curvature corresponds to a positive moment and is plotted on the tension side of the beam. For all test units and all load levels the negative curvatures were considerably larger than the positive curvatures. The positive curvatures were spread over a larger length of the beam than the negative curvatures, which were concentrated at the end of the spandrel. This corresponds to the observation that the length of the positive plastic was larger than the length of the negative plastic hinge.

For TU5, i.e. the test unit with the smallest longitudinal reinforcement content, the maximum positive curvatures occurred well inside the span of the spandrel. Note that for larger rotations the curvature pattern is not as clear as for smaller rotations due to the plastic deformations in previous cycles. For TU3, which had an intermediate longitudinal reinforcement content, in particular for the positive direction of loading, a clear shift of the positive plastic hinge towards the edge of the spandrel for increasing rotation demands can be observed, which is deemed associated with the continuous crushing of the compression diagonal strut. For TU4 the curvatures for the cycles with $\sigma=0.4$ MPa were smaller than the yield curvature. The negative curvature was concentrated at the end of the spandrel while the maximum positive curvature was just inside the spandrel. Once the axial stress in the piers was increased to $\sigma=0.6$ MPa the negative hinges yielded while the positive hinges reached just about the estimated yield curvature.

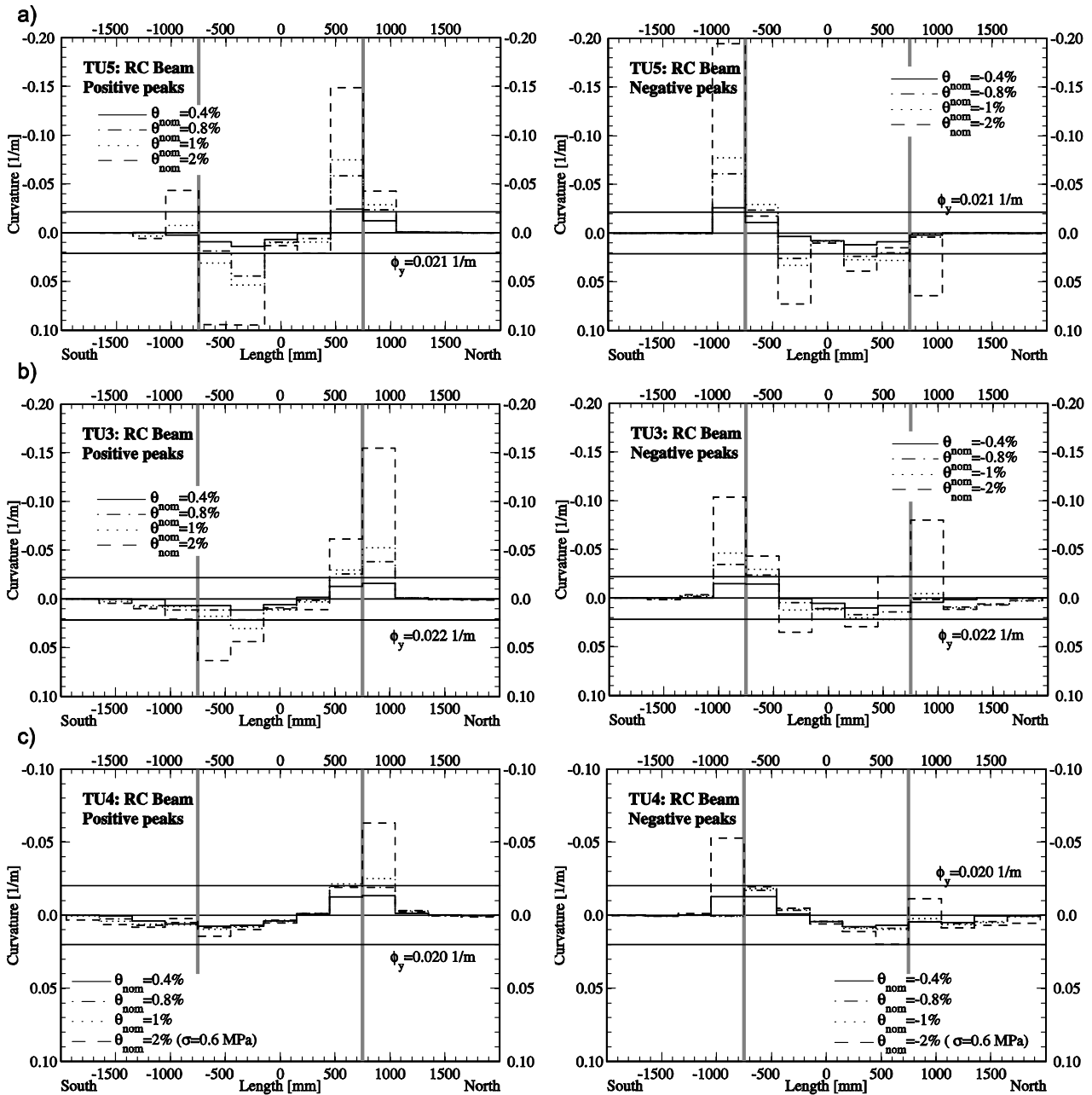


Figure 7. Curvature distribution along the RC beam for selected cycles with positive drift demand (left column) and negative drift demand (right column). The solid vertical lines clear the free span of the spandrel.

Summary and Conclusions

Composite spandrel elements consisting of a masonry spandrel and a RC ring beam contribute to the in-plane strength of URM walls. Quasi-static cyclic tests on composite

spandrel elements have shown the influence of the longitudinal reinforcement content on the behavior of the composite spandrel in terms of failure mechanism, force and deformation capacity, hysteretic behavior and curvature demand on the RC beam. Although the RC beams had larger shear reinforcement ratios than required by the Italian seismic design code [OPCM 2003, 2005], which propagates the use of RC ring beams in URM buildings, two of the three beams failed in shear. One reason for this is that the assumed mechanism that was observed during the tests of the composite spandrel does not correspond exactly to the mechanisms assumed by design guidelines (see [Beyer 2011] for details). Based on these preliminary results it is recommended to compute the shear demand as $V=2M_{pl}/(0.67l_{sp})$ where M_{pl} is the moment capacity of the RC beam.

Future work will include the in-depth analysis of the optical measurement data as well as the development of numerical and mechanical models for composite spandrels. One first numerical model and its results are presented in the companion paper [Beyer 2011].

References

- Beyer 2010a: Beyer, K., A. Abo-El-Ezz, A. Dazio, "Quasi-static cyclic tests on different types of masonry spandrels," Technical report, Institute of Structural Engineering, ETH Zurich, Switzerland, 2010.
- Beyer 2010b: Beyer, K., A. Dazio "Quasi-static cyclic tests on masonry spandrels", submitted to Earthquake Spectra, 2010.
- Beyer 2011: Beyer, K., A. Dazio, "Experimental investigation of the longitudinal reinforcement content of ring beams on the cyclic behaviour of masonry spandrels," Proceedings of the 11th North American Masonry Conference, Minneapolis, 2011.
- CEN 2005: CEN, Eurocode 8: Design of structures for earthquake resistance – Part 3: General rules, seismic actions and rules for buildings, Design Code EN 1998-3, European Committee for Standardisation, Brussels, Belgium, 2005.
- Frumento 2009: Frumento, S., G. Magenes, P. Morandi, G.M. Calvi "Interpretation of experimental shear tests on clay brick masonry walls and evaluation of q-factors for seismic design," Technical report 2009/02, IUSS Press, EUCENTRE and University of Pavia, Italy, 2009.
- Milani 2009: Milani, G., K. Beyer, A. Dazio "Upper bound limit analysis of meso-mechanical spandrel models for the pushover analysis of 2D masonry frames," Engineering Structures 31 (11), 2009, pp. 2696-2710.
- NDI 2009: NDI, Optotrak Certus HD, Northern Digital Inc., Waterloo, Ontario, Canada, 2009, <http://www.ndigital.com/industrial/certushd.php>.
- OPCM 2003: O.P.C.M. 3274, 20/03/2003. First elements concerning general criteria for the seismic classification of the national territory and technical norms for structures in seismic zone" (in Italian), Design Code OPCM 3274, 2003.
- OPCM 2005: O.P.C.M. 3431/05, 09/05/2005. Further modifications and integrations on OPCM 3274/03" (in Italian), Design Code OPCAM 3431/05, 2005.
- Priestley 2007: Priestley, M.J.N., G.M. Calvi, M.J. Kowalsky, Displacement-based seismic design of structures, IUSS Press, Pavia, Italy, 2007.